Photocarrier thermalization bottleneck in graphene

Dinesh Yadav,[1,2] Maxim Trushin,[3] and Fabian Pauly[1,2]
[1]*Okinawa Institute of Science and Technology Graduate University, Onna-son, Okinawa 904-0495, Japan*
[2]*Department of Physics, University of Konstanz, 78457 Konstanz, Germany*
[3]*Centre for Advanced 2D Materials, National University of Singapore, 6 Science Drive 2, Singapore 117546*

(Received 20 April 2018; revised manuscript received 26 January 2019; published 8 April 2019)

We present a theoretical study of photocarrier dynamics in graphene due to electron-phonon (EP) interactions. Using the relaxation-time approximation (RTA) with parameters determined from density functional theory (DFT) and a complementary explicitly solvable model, we show that the photocarrier thermalization time changes by orders of magnitude, when the excitation energy is reduced from 1 eV to the 100 meV range. In detail the ultrafast thermalization at low temperatures takes place on a femtosecond timescale via optical phonon emission, but slows down to picoseconds once excitation energies become comparable with these optical phonon energy quanta. In the latter regime thermalization times exhibit a pronounced dependence on temperature. Our DFT-based model includes all the inter- and intraband transitions due to EP scattering. Thanks to the high melting point of graphene we extend our studies up to 2000 K and show that such high temperatures reduce the photocarrier thermalization time through phonon absorption.

DOI: 10.1103/PhysRevB.99.155410

I. INTRODUCTION

Recent progress in nanotechnology has made it possible to fabricate high-quality materials that are only one atom thick and hence reach the fundamental two-dimensional (2D) limit for solid crystals [1]. Due to their ultimate thinness these materials demonstrate various properties that are qualitatively different from those of the three-dimensional parent crystals and, at the same time, are found to be useful in photodetection and photovoltaic applications [2]. Indeed, the central phenomenon employed in photodetection and photovoltaics is the conversion of light energy into electricity. It is a quantum conversion process, employing absorption of photons to deliver photoexcited carriers to an external circuit, where they do electrical work [3]. There are two obvious strategies for increasing the amount of energy transferred by photocarriers. One can try to speed up the photocarrier extraction such that the carriers are collected, while they are still hot or even out of thermal equilibrium. Alternatively, one can try to slow down the cooling or photocarrier thermalization for the same purpose.

Graphene in a combination with other 2D semiconductors offers an interesting opportunity to employ both strategies. Thanks to the extremely small thickness of the junctions between 2D materials (also known as van der Waals heterostructures [4]), interlayer photocarrier transport may occur faster than the intralayer relaxation processes [5]. At the same time the optical phonon emission is strongly suppressed for low-energy excitations in graphene due to unusually high energy quanta of optical phonons [6,7]. As a consequence, the photocarriers can be extracted well before they thermalize and dissipate useful energy by means of phonon emission. By incorporating graphene into a heterostructure, we can combine the two strategies in one optoelectronic device. In this way the photoresponse can be substantially increased simultaneously to the device performance. In this paper we focus on the photocarrier evolution in intrinsic graphene, providing conclusive evidence for the existence of a thermalization bottleneck that makes such applications possible.

The striking difference between electron thermalization in intrinsic graphene and in a metal (e.g., doped graphene) is that the electron-electron collision rate is much lower in the former than in the latter, as it has been pointed out and confirmed by means of Raman spectroscopy by Basko *et al.* [8]. Indeed two electrons colliding with each other have to satisfy energy and momentum conservation. If one electron is excited in the conduction band, then it most likely collides with another electron from the valence band (interband electron-electron scattering), as the conduction band is almost empty in intrinsic graphene. The only possible way to satisfy both conservation laws in this case is to assume all four involved momenta to be parallel (collinear scattering). This is a direct consequence of the conelike dispersion for carriers in graphene. Other collinear channels involved in the electron-electron scattering are Auger recombination and carrier multiplication. Both lead to a change in the excited charge carrier density [9–14]. Carrier multiplication is favorable at low pump fluence and high excitation energies, whereas Auger recombination requires high pump fluence and low excitation energies [9,11,15]. Furthermore, these processes are very sensitive to the doping level and temperature [13–16]. Collinear scattering is an inefficient thermalization mechanism, and the corresponding electron-electron thermalization time is about 1 ps for photocarriers excited in the optical spectral region, and it is even longer for lower excitation energies [6,7,17]. Since our model is developed to provide a solid proof for the photocarrier thermalization bottleneck in intrinsic graphene that occurs at the excitation energy near 100 meV, the electron-electron scattering turns out to be irrelevant for such excitation energies and only EP scattering is taken into account. This assumption is

invalid for conventional heavily doped graphene samples with a Fermi energy of about 200 meV. However, such samples would not be suitable for studying the photocarrier thermalization bottleneck, as the relevant interband excitations are blocked by the Pauli principle.

In contrast to advanced two-temperature models for electron thermalization in metals [18–20] and semiconductors [21] we are dealing here with a single temperature describing both the thermalized electrons and equilibrium phonons. This single-temperature model does not treat the thermalization of phonons, which would require us to take into account additional effects such as phonon-phonon scattering due to anharmonicities [22]. Neglecting weak perturbations from nonequilibrium phonon occupations, the photoexcited electrons in our model relax directly to the Fermi-Dirac distribution that is already in thermal equilibrium with the phonon bath. The temperature can be much higher than 300 K due to sample heating, but we assume the absorbed radiation fluence to be low enough to prevent a further increase of this temperature.

The photocarrier dynamics in graphene has been studied experimentally by means of pump-probe spectroscopy as well as time- and angle-resolved photoemission spectroscopy [23–31]. In the experiments the carriers are excited far above the Dirac point (by more than 1 eV), and the ultrafast relaxation of hot carriers is mainly attributed to optical phonon emission and electron-electron scattering, taking place within 150–170 fs [23,28]. Excitations below the highest optical phonon energy (of around 200 meV in graphene) have been studied in Refs. [6,7,32], where it has been observed that the relaxation time is drastically increased from the femtosecond to the picosecond timescale. There has been a number of theoretical attempts to understand the thermalization and cooling in graphene [6,14,33–42], but most of the models suffer from drawbacks by neglecting the acoustical phonons or the contribution from other points in the Brillouin zone (BZ). EP coupling in n-doped graphene has been studied using *ab-initio* methods but not for the intrinsic graphene [43]. Further Raman spectroscopy has revealed the complex nature of the phonon dynamics in the presence of hot carriers [44,45].

Our approach extracts the leading mechanism responsible for the suppression of the photocarrier thermalization at low excitation energy and provides an explicitly solvable model for further insights. In detail we present an *ab-initio* method to calculate the band and momentum resolved scattering times $\tau_{n\mathbf{k}}(T)$ along with their temperature dependence. We use $\tau_{n\mathbf{k}}(T)$ in the Boltzmann equation under the RTA to calculate the thermalization time $\tau_{\rm th}$. Inclusion of contributions arising from all the optical and acoustical phonon branches in the whole BZ makes it possible to calculate precisely the relaxation time without adjustable parameters. Moreover, we include inter- and intraband processes due to EP scattering. We investigate the relaxation time for different excitation energies from 0.05 to 0.8 eV and over a wide range of temperatures from 0 to 2000 K taking advantage of the high melting point of graphene [46].

Our paper is organized as follows. In Sec. II we present the theoretical approaches used in this work. Next, we discuss the results obtained within the models in Sec. III before we end with a summary and outlook in Sec. IV.

II. THEORETICAL APPROACHES

In this section we describe the theoretical approaches that we apply. In Sec. II A these are the details of our DFT calculations to determine electronic and phononic properties. Subsequently, we present in Sec. II B the Boltzmann equations in the RTA, as employed to determine the photocarrier dynamics. In Sec. II C we finally discuss simplifications to the RTA in order to obtain an explicitly solvable model.

A. *Ab-initio* theory for electronic and phononic properties

We use DFT within the local density approximation (LDA) to calculate the ground-state electronic properties of graphene with QUANTUM ESPRESSO [47]. We employ a plane-wave basis set with a kinetic energy cutoff of 110 Ry, a charge density cutoff of 440 Ry and a Troullier-Martins pseudopotential for carbon with a $2s^2 2p^2$ valence configuration [48]. The unit cell of graphene is relaxed with the help of the Broyden-Fletcher-Goldfarb-Shanno algorithm until the net force on atoms is less than 10^{-6} Ry/a.u., and total energy changes are below 10^{-8} Ry. A vacuum of 20 Å along the out-of-plane direction is used to avoid artificial interactions with periodic images of the graphene sheet, and the BZ is sampled with a $45\times45\times1$ Γ-centered $\mathbf{k}$ grid. We construct Wannier functions to get localized orbitals from plane-wave eigenfunctions. By interpolating wave functions, we finally obtain electronic eigenenergies, dynamical matrices, and EP couplings on fine grids in the BZ [49]. We calculate the phonon dispersion spectrum of graphene through density functional perturbation theory (DFPT) [50], employing a $12\times12\times1$ $\mathbf{q}$ grid to evaluate phonon dynamical matrices.

By performing the DFT procedures, we obtain an optimized in-plane lattice constant of graphene of $a = |\mathbf{a}_1| = |\mathbf{a}_2| = 2.436$ Å, see Fig. 1(a), which is in good agreement with previous reports of 2.458 Å [51]. We calculate electronic and phononic band structures along high symmetry lines of the first BZ, as plotted in Fig. 1(b). Figure 1(c) shows the electronic band structure, as computed from DFT with plane waves. The excellent agreement with those determined through the Wannier function method demonstrates the high quality of the interpolated localized orbitals. The phonon dispersion is finally displayed in Fig. 1(d). Longitudinal optical and transverse optical phonon modes of graphene at the Γ point are degenerate at an energy of 198.37 meV, which matches well with a previously reported value of 197.75 meV [51].

Having determined electronic and phononic band structures, we calculate the electronic self-energy $\Sigma_{n\mathbf{k}}(T)$ due to the EP interaction for the electronic eigenstate $|n\mathbf{k}\rangle$ with the EPW code. It is defined as follows [52]:

$$\Sigma_{n\mathbf{k}}(T) = \sum_{m,p} \int_{\rm BZ} \frac{d^3q}{\Omega_{\rm BZ}} |g_{mn,p}(\mathbf{k},\mathbf{q})|^2 \times \left[\frac{N_{\hbar\omega_{p\mathbf{q}}}(T) + f^{(0)}_{\varepsilon_{m\mathbf{k}+\mathbf{q}}}(T)}{\varepsilon_{n\mathbf{k}} - (\varepsilon_{m\mathbf{k}+\mathbf{q}} - \varepsilon_{\rm F}) + \hbar\omega_{p\mathbf{q}} + i\eta} + \frac{N_{\hbar\omega_{p\mathbf{q}}}(T) + 1 - f^{(0)}_{\varepsilon_{m\mathbf{k}+\mathbf{q}}}(T)}{\varepsilon_{n\mathbf{k}} - (\varepsilon_{m\mathbf{k}+\mathbf{q}} - \varepsilon_{\rm F}) - \hbar\omega_{p\mathbf{q}} + i\eta} \right], \quad (1)$$

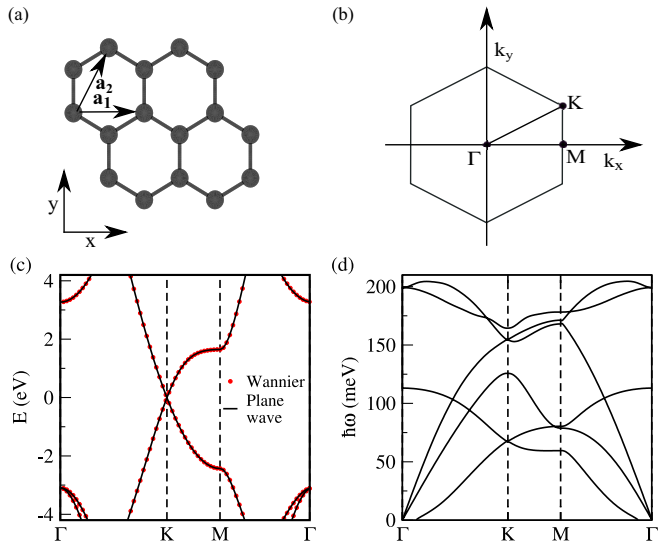

FIG. 1. (a) Lattice structure of graphene with in-plane lattice vectors $\mathbf{a}_1$ and $\mathbf{a}_2$. (b) Reciprocal lattice of graphene with high symmetry points in the first BZ. (c) Electronic band structure of graphene, as obtained directly from the calculations with the plane-wave basis set and the corresponding curve from the Wannier-function formalism. (d) Phonon band structure of graphene.

where n is the band index, $\mathbf{k}$ is an electronic wave vector in the BZ, $\hbar\omega_{p\mathbf{q}}$ is the energy of the phonon of branch p at wave vector $\mathbf{q}$, $\varepsilon_F = 0$ is the Fermi energy, $f^{(0)}_{\varepsilon_{n\mathbf{k}}}(T) = 1/[\exp(\frac{\varepsilon_{n\mathbf{k}}-\varepsilon_F}{k_B T}) + 1]$ is the Fermi-Dirac distribution, $N_{\hbar\omega_{p\mathbf{q}}}(T) = 1/[\exp(\frac{\hbar\omega_{p\mathbf{q}}}{k_B T}) - 1]$ is the Bose function, Ω_{BZ} is the volume of the BZ, and $\eta = 10$ meV is the small broadening parameter. The EP matrix elements are defined as [52]

$$g_{mn,p}(\mathbf{k},\mathbf{q}) = \frac{1}{\sqrt{2\omega_{p\mathbf{q}}}}\langle m\mathbf{k}+\mathbf{q}|\partial_{p\mathbf{q}}V|n\mathbf{k}\rangle \tag{2}$$

and provide information about the scattering processes happening between the Kohn-Sham states $|m\mathbf{k}+\mathbf{q}\rangle$ and $|n\mathbf{k}\rangle$, as mediated by the derivative $\partial_{p\mathbf{q}}V$ of the self-consistent Kohn-Sham potential with respect to the phonon wave vector $\mathbf{q}$ in branch p. Note that we assume that electron and phonon baths are at the same temperature T. The first term in the brackets of Eq. (1) can be seen as arising from absorption of phonons and the second one from their emission.

To obtain converged results for Eq. (1), we first calculate the electronic and vibrational states on a $36\times36\times1$ $\mathbf{k}$ grid and a $12\times12\times1$ $\mathbf{q}$ grid using DFT and DFPT with plane-wave basis functions [47], respectively. Finally, the electron eigenenergies, wave functions, and phonon dynamical matrices are interpolated on fine grids using Wannier functions [53]. We use a $1200\times1200\times1$ $\mathbf{k}$ grid and a $300\times300\times1$ $\mathbf{q}$ grid, which we find necessary to accurately map out the whole BZ and to converge the integral over $\mathbf{q}$ in Eq. (1).

We assume that electronic wave functions and phonon dynamical matrices do not change with EP interactions [52]. Furthermore, there are no anharmonic effects that change the scattering rates and renormalize phonon frequencies [22]. The EP scattering time, resolved according to the electronic band and momentum, is calculated as

$$\tau_{n\mathbf{k}}(T) = \frac{\hbar}{2\mathrm{Im}[\Sigma_{n\mathbf{k}}(T)]} \tag{3}$$

from Eq. (1) by using the imaginary part of the self-energy.

B. Time evolution of excited charge carriers

The time evolution of the electronic occupation $\tilde{f}_{n\mathbf{k}}(t,T)$ is calculated using the Boltzmann equation in the RTA

$$\frac{d\tilde{f}_{n\mathbf{k}}(t,T)}{dt} = -\frac{\tilde{f}_{n\mathbf{k}}(t,T) - f^{(0)}_{\varepsilon_{n\mathbf{k}}}(T)}{\tau_{n\mathbf{k}}} \tag{4}$$

with the solution

$$\tilde{f}_{n\mathbf{k}}(t,T) = f^{(0)}_{\varepsilon_{n\mathbf{k}}}(T) + e^{-\frac{t}{\tau_{n\mathbf{k}}}}\left[\tilde{f}_{n\mathbf{k}}(0,T) - f^{(0)}_{\varepsilon_{n\mathbf{k}}}(T)\right], \tag{5}$$

if the excitation is assumed to happen at time $t = 0$. Equation (5) states that when the system is weakly perturbed, the perturbation decays exponentially with the scattering time $\tau_{n\mathbf{k}}$ to restore the equilibrium Fermi-Dirac distribution $f^{(0)}_{\varepsilon_{n\mathbf{k}}}(T)$ [54]. RTA omits all the intermediate relaxation steps between an initial nonequilibrium electron distribution and its final relaxed occupation so that an excited electron relaxes directly to the thermalized state. It is valid only when the system is weakly perturbed from the equilibrium and higher order perturbations can be safely neglected. We consider here the isotropic scattering processes only, i.e., there is no angular dependence and $\tau_{n\mathbf{k}}$ is the average time between the EP collision events. The tilde sign indicates the time dependence of the occupation function.

We generate the initial hot-carrier occupation $\tilde{f}_{n\mathbf{k}}(0,T)$ as a combination of a Fermi-Dirac distribution $f^{(0)}_{\varepsilon_{n\mathbf{k}}}(T)$ at the temperature T and a Gaussian peak at energy $+\zeta$ for electrons in the conduction band ($\varepsilon_{n\mathbf{k}} > \varepsilon_F$) and $-\zeta$ for the holes in the valence band ($\varepsilon_{n\mathbf{k}} < \varepsilon_F$) as

$$\tilde{f}_{n\mathbf{k}}(0,T) = f^{(0)}_{\varepsilon_{n\mathbf{k}}}(T)\begin{cases} +\frac{\lambda_e}{\sqrt{2\pi\sigma^2}}e^{\frac{(\varepsilon_{n\mathbf{k}}-\zeta)^2}{2\sigma^2}}, & \varepsilon_{n\mathbf{k}} \geqslant \varepsilon_F, \\ -\frac{\lambda_h}{\sqrt{2\pi\sigma^2}}e^{\frac{(\varepsilon_{n\mathbf{k}}+\zeta)^2}{2\sigma^2}}, & \varepsilon_{n\mathbf{k}} < \varepsilon_F. \end{cases} \tag{6}$$

Throughout this work we choose a small energy smearing $\sigma = 8.47$ meV and small perturbation $\lambda_e = 2.4\times10^{-3}$ eV. The parameter λ_h is selected such that the initially excited number of electrons and holes is the same. Since the density of states (DOS) of graphene is rather symmetric in the range of excitation energies $-0.8 \leqslant \zeta \leqslant 0.8$ eV studied by us [see Fig. 1(c)], it turns out to be an excellent approximation to set $\lambda = \lambda_e = \lambda_h$.

While we use λ here as a free parameter to adjust the initial occupation, it can be related to measurements through $\lambda = 4\pi^2\alpha\hbar^2\Phi v_F^2/\zeta^2$. In the expression, $\pi\alpha$ is the linear absorption of graphene, Φ is the pump-fluence, and v_F is the Fermi velocity of electrons in graphene [17].

We determine the time τ_{th} when hot carriers have relaxed through the relation $P(\zeta,0,T) - P(\zeta,t,T) < P(\zeta,0,T)/e$. In the expression we have defined the population

$$P(E,t,T) = \sum_{n\mathbf{k}}\delta(E-\varepsilon_{n\mathbf{k}})\begin{cases}[1-\tilde{f}_{n\mathbf{k}}(t,T)], & E < \varepsilon_F, \\ \tilde{f}_{n\mathbf{k}}(t,T), & E \geqslant \varepsilon_F. \end{cases} \tag{7}$$

Our definition ensures that the population is symmetric with regard to electrons and holes, as long as the DOS is symmetric.

C. Analytical model

Before performing parameter-free *ab-initio* calculations of charge carrier dynamics, we estimate the photocarrier thermalization time of intrinsic graphene within an explicitly solvable model. For simplicity we assume only optical phonon modes p that are dispersionless, i.e., exhibit the fixed energy $\hbar\omega_p$. For this reason phonon wave vectors will be omitted. Furthermore, we consider only the two linear electronic bands of the Dirac cone with $\varepsilon_{n\mathbf{k}} = n\hbar v_F k$, $n = \pm$ and $k = |\mathbf{k}|$. Additionally, we will suppress all time and temperature arguments of the occupation functions in this subsection, because we assume a steady state regime.

The EP collisions in the given optical phonon mode p are governed by the following integral:

$$I_p[\tilde{f}_{n\mathbf{k}}] = \sum_{n'\mathbf{k}'} [\tilde{f}_{n'\mathbf{k}'}(1-\tilde{f}_{n\mathbf{k}})W_{n'\mathbf{k}'\to n\mathbf{k}} - \tilde{f}_{n\mathbf{k}}(1-\tilde{f}_{n'\mathbf{k}'})W_{n\mathbf{k}\to n'\mathbf{k}'}], \tag{8}$$

where $\tilde{f}_{n\mathbf{k}} = f^{(0)}_{\varepsilon_{n\mathbf{k}}} + \tilde{f}^{(1)}_{n\mathbf{k}}$ denotes the carrier occupation with the time-independent Fermi-Dirac distribution $f^{(0)}_{\varepsilon_{n\mathbf{k}}}$ and the nonequilibrium addition $\tilde{f}^{(1)}_{n\mathbf{k}}$, representing the second term in Eq. (5). The transition probability is given by Fermi's golden rule

$$W_{n\mathbf{k}\to n'\mathbf{k}'} = \frac{2\pi}{\hbar} W_p[(N_p+1)\delta(\varepsilon_{n\mathbf{k}} - \varepsilon_{n'\mathbf{k}'} - \hbar\omega_p) + N_p\delta(\varepsilon_{n\mathbf{k}} - \varepsilon_{n'\mathbf{k}'} + \hbar\omega_p)] \tag{9}$$

for carriers outgoing from the state $|n\mathbf{k}\rangle$, and

$$W_{n'\mathbf{k}'\to n\mathbf{k}} = \frac{2\pi}{\hbar} W_p[(N_p+1)\delta(\varepsilon_{n'\mathbf{k}'} - \varepsilon_{n\mathbf{k}} - \hbar\omega_p) + N_p\delta(\varepsilon_{n'\mathbf{k}'} - \varepsilon_{n\mathbf{k}} + \hbar\omega_p)] \tag{10}$$

for carriers incoming to the state $|n\mathbf{k}\rangle$. Making use of nearly dispersionless optical phonon modes, the EP interaction matrix element W_p is assumed to be independent of momentum. The first term in both Eqs. (9) and (10) corresponds to the phonon emission, while the second one describes the phonon absorption. The phonons are treated as a noninteracting gas, characterized by the Bose-Einstein distribution $N_p = N_{\hbar\omega_p}(T)$. Due to the strong carbon-carbon bonding in graphene the optical phonon energy is higher than 100 meV [see Fig. 1(c)] and, hence, we assume $\hbar\omega_p \gg k_B T$ for typical temperatures or, in other words, $N_p \ll 1$. The collision integral can then be simplified to

$$I_p[\tilde{f}_{n\mathbf{k}}] = \frac{2\pi}{\hbar} W_p \sum_{n'\mathbf{k}'} [\tilde{f}_{n'\mathbf{k}'}(1-\tilde{f}_{n\mathbf{k}})\delta(\varepsilon_{n'\mathbf{k}'} - \varepsilon_{n\mathbf{k}} - \hbar\omega_p) - \tilde{f}_{n\mathbf{k}}(1-\tilde{f}_{n'\mathbf{k}'})\delta(\varepsilon_{n\mathbf{k}} - \varepsilon_{n'\mathbf{k}'} - \hbar\omega_p)]. \tag{11}$$

Let us now assume $\tilde{f}_{n\mathbf{k}}$ to be a function of $\varepsilon_{n\mathbf{k}}$ and integrate in momentum space. Making use of the δ function and $\varepsilon_{nk} = \varepsilon_{n\mathbf{k}}$, we obtain

$$I_p\big[\tilde{f}_{\varepsilon_{nk}}\big] = \frac{W_p}{\hbar^3 v_F^2}\big[|\varepsilon_{nk} + \hbar\omega_p|\tilde{f}_{\varepsilon_{nk}+\hbar\omega_p}\big(1-\tilde{f}_{\varepsilon_{nk}}\big) - |\varepsilon_{nk} - \hbar\omega_p|\tilde{f}_{\varepsilon_{nk}}\big(1-\tilde{f}_{\varepsilon_{nk}-\hbar\omega_p}\big)\big]. \tag{12}$$

Finally, we employ a linear response approximation and the property of intrinsic graphene $1 - f^{(0)}_{\varepsilon_{nk}} = f^{(0)}_{-\varepsilon_{nk}}$ so that

$$\tilde{f}_{\varepsilon_{nk}+\hbar\omega_p}\big(1-\tilde{f}_{\varepsilon_{nk}}\big) \approx f^{(0)}_{\varepsilon_{nk}+\hbar\omega_p} f^{(0)}_{-\varepsilon_{nk}} - \tilde{f}^{(1)}_{\varepsilon_{nk}} f^{(0)}_{\varepsilon_{nk}+\hbar\omega_p} + \tilde{f}^{(1)}_{\varepsilon_{nk}+\hbar\omega_p} f^{(0)}_{-\varepsilon_{nk}}, \tag{13}$$

$$\tilde{f}_{\varepsilon_{nk}}\big(1-\tilde{f}_{\varepsilon_{nk}-\hbar\omega_p}\big) \approx f^{(0)}_{-\varepsilon_{nk}+\hbar\omega_p} f^{(0)}_{\varepsilon_{nk}} + \tilde{f}^{(1)}_{\varepsilon_{nk}} f^{(0)}_{-\varepsilon_{nk}+\hbar\omega_p} - \tilde{f}^{(1)}_{\varepsilon_{nk}-\hbar\omega_p} f^{(0)}_{\varepsilon_{nk}}. \tag{14}$$

Hence, Eq. (12) can be written as a sum of two terms $I_p[\tilde{f}_{\varepsilon_{nk}}] = I_p[f^{(0)}_{\varepsilon_{nk}}] + \hat{I}_p[f^{(0)}_{\varepsilon_{nk}}, \tilde{f}^{(1)}_{\varepsilon_{nk}}]$, where

$$I_p\big[f^{(0)}_{\varepsilon_{nk}}\big] = \frac{W_p}{\hbar^3 v_F^2}\Big[|\varepsilon_{nk} + \hbar\omega_p| f^{(0)}_{\varepsilon_{nk}+\hbar\omega_p} f^{(0)}_{-\varepsilon_{nk}} - |\varepsilon_{nk} - \hbar\omega_p| f^{(0)}_{-\varepsilon_{nk}+\hbar\omega_p} f^{(0)}_{\varepsilon_{nk}}\Big], \tag{15}$$

$$\hat{I}_p\big[f^{(0)}_{\varepsilon_{nk}}, \tilde{f}^{(1)}_{\varepsilon_{nk}}\big] = \frac{W_p}{\hbar^3 v_F^2}\Big[|\varepsilon_{nk} + \hbar\omega_p|\Big(\tilde{f}^{(1)}_{\varepsilon_{nk}+\hbar\omega_p} f^{(0)}_{-\varepsilon_{nk}} - \tilde{f}^{(1)}_{\varepsilon_{nk}} f^{(0)}_{\varepsilon_{nk}+\hbar\omega_p}\Big) - |\varepsilon_{nk} - \hbar\omega_p|\Big(\tilde{f}^{(1)}_{\varepsilon_{nk}} f^{(0)}_{-\varepsilon_{nk}+\hbar\omega_p} - \tilde{f}^{(1)}_{\varepsilon_{nk}-\hbar\omega_p} f^{(0)}_{\varepsilon_{nk}}\Big)\Big]. \tag{16}$$

Equations (15) and (16) are valid for any ratio between ε_{nk} and $\hbar\omega_p$ so that we can investigate the thermalization behavior for photocarriers excited below and above the phonon frequency. Note that only Eq. (16) is responsible for thermalization, because Eq. (15) does not contain $\tilde{f}^{(1)}_{\varepsilon_{nk}}$.

In what follows we consider the thermalization of electrons (i.e., $\varepsilon_k = \varepsilon_{+k} = \hbar v_F k$), as the thermalization of holes is equivalent in the case of intrinsic graphene at not too high excitation energies [see Fig. 1(c)]. Assuming the initial nonequilibrium distribution to be δ shaped, $f^{(1)}_{\varepsilon_k} \propto \delta(\varepsilon_k - \hbar\omega/2)$, we find

$$I_p\big[\tilde{f}_{\varepsilon_k}\big] = \frac{\omega W_p}{2\hbar^2 v_F^2}\Big(\tilde{f}^{(1)}_{\varepsilon_k+\hbar\omega_p} f^{(0)}_{-\frac{\hbar\omega}{2}+\hbar\omega_p} + \tilde{f}^{(1)}_{\varepsilon_k-\hbar\omega_p} f^{(0)}_{\frac{\hbar\omega}{2}+\hbar\omega_p}\Big) - \frac{W_p}{\hbar^2 v_F^2}\tilde{f}^{(1)}_{\varepsilon_k}\Big(\Big|\frac{\omega}{2}+\omega_p\Big| f^{(0)}_{\frac{\hbar\omega}{2}+\hbar\omega_p} + \Big|\frac{\omega}{2}-\omega_p\Big| f^{(0)}_{-\frac{\hbar\omega}{2}+\hbar\omega_p}\Big). \tag{17}$$

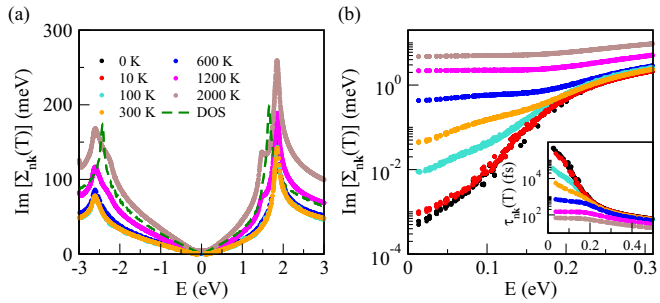

FIG. 2. (a) Imaginary part of the EP self-energy as a function of energy, evaluated at different temperatures, and the electronic DOS of graphene. (b) Zoom in on the energy and temperature dependence of $\mathrm{Im}[\Sigma_{n\mathbf{k}}(T)]$. We consider only positive energies close to the Dirac point. The inset represents the corresponding scattering times.

Equation (17) contains cascade terms, generated each time, when a phonon is emitted or absorbed [37]. We use the RTA, i.e., we truncate the cascade to a single term proportional to $\tilde{f}_{\varepsilon}^{(1)}$. This results in the thermalization time given by

$$\frac{1}{\tau_{\mathrm{th}}} = \sum_{p} \frac{W_p}{\hbar^2 v_{\mathrm{F}}^2} \left(\left| \frac{\omega}{2} + \omega_p \right| f^{(0)}_{\frac{\hbar\omega}{2}+\hbar\omega_p} + \left| \frac{\omega}{2} - \omega_p \right| f^{(0)}_{-\frac{\hbar\omega}{2}+\hbar\omega_p} \right). \tag{18}$$

This analytical model is of course not able to give quantitative predictions, but it suggests that the thermalization time at $\omega_p \gg \omega/2$ is much longer than at $\omega_p \ll \omega/2$. Indeed, in the latter limit we have

$$\frac{1}{\tau_{\mathrm{th}}} = \sum_{p} \frac{\omega W_p}{2\hbar^2 v_{\mathrm{F}}^2}, \quad \omega_p \ll \omega/2, \tag{19}$$

whereas in the former case the rate contains an exponentially small multiplier, resulting in the following expression:

$$\frac{1}{\tau_{\mathrm{th}}} = \sum_{p} \frac{2\omega_p W_p}{\hbar^2 v_{\mathrm{F}}^2} e^{-\frac{\hbar\omega_p}{k_{\mathrm{B}}T}}, \quad \omega_p \gg \omega/2. \tag{20}$$

We will confirm the predictions of Eqs. (19) and (20) in the next section using the *ab-initio* approach. Note, however, that while the approximation $\hbar\omega_p \gg k_{\mathrm{B}}T$ or $N_p \ll 1$, made for their derivation, is excellent for most temperatures studied, we will consider temperatures of up to 2000 K with our *ab-initio* approach, where this approximation becomes questionable.

III. RESULTS

We will now use the *ab-initio* parameters for electrons, phonons, and their couplings, determined as described in Sec. II A, and combine them with the Boltzmann formalism of Sec. II B to study photocarrier thermalization. At the end we will compare to the results of the analytical equations as derived in Sec. II C.

Since we determine scattering times $\tau_{n\mathbf{k}}$ of the Boltzmann formalism [see Eq. (4)] from the imaginary part of the EP self-energy [see Eq. (1)], we investigate this quantity first. Figure 2(a) plots $\mathrm{Im}[\Sigma_{n\mathbf{k}}(T)]$ as a function of energy for different temperatures. For a given temperature it shows a pronounced energy dependence. Increasing initially monotonically and rather symmetrically in the vicinity of the Dirac point at $E = \varepsilon_{\mathrm{F}} = 0$, it follows the same behavior as the electronic DOS [see Eq. (1)]. This results from the fact that the electronic DOS represents the phase space for EP scattering events to take place. As can be inferred from Figs. 2(a) and 2(b), $\mathrm{Im}[\Sigma_{n\mathbf{k}}(T)]$ is very sensitive to temperature close to $E = 0$. In contrast it shows a much weaker temperature dependence at energies above around 200 meV, coinciding with the highest optical phonon energies. Indeed, we see for low temperatures (0–300 K) that $\mathrm{Im}(\Sigma_{n\mathbf{k}})$ increases roughly exponentially until the highest optical phonon energy is reached, while the energy dependence is comparatively weak for elevated temperatures (600–2000 K). The behavior shows that scattering below the optical phonon threshold takes place rather inefficiently via acoustical phonons. With increasing temperature there are more phonons available for the carriers to interact with, leading to the increase of $\mathrm{Im}[\Sigma_{n\mathbf{k}}(T)]$. Analogously, the available phase space for optical phonon emission grows with increasing energy.

In the inset of Fig. 2(b) we consider the scattering times $\tau_{n\mathbf{k}}(T)$, which are inversely proportional to the self-energy [see Eq. (3)]. We observe that around the Dirac point the scattering time becomes very sensitive to temperature and can be on the order of a few picoseconds for low T. In contrast, at energies above 200 meV the scattering times exhibit only weak energy and temperature dependencies. As argued before, this behavior can be rationalized by the fact that for low T at $E < 200$ meV excited carriers can relax via acoustical phonon scattering only, while they thermalize efficiently via optical phonons above 200 meV.

The behavior of $\mathrm{Im}[\Sigma_{n\mathbf{k}}(T)]$ in Fig. 2 can also be analyzed in terms of Eq. (1). Lets consider low temperatures and electrons with $\varepsilon_{n\mathbf{k}} \geqslant 0$. In this case both $f^{(0)}_{\varepsilon_{n\mathbf{k}}}(T)$ and $N_{\hbar\omega_{p\mathbf{q}}}(T)$ are vanishingly small, and thus only the second term of Eq. (1) contributes. For this reason, excited electrons relax via emission of phonons. But as temperature increases, we get $0 \leqslant f^{(0)}_{\varepsilon_{n\mathbf{k}}}(T) \leqslant 1$ and $N_{\hbar\omega_{p\mathbf{q}}}(T) > 0$, and both terms in Eq. (1) start contributing. For this reason $\mathrm{Im}[\Sigma_{n\mathbf{k}}(T)]$ increases with increasing temperature in Fig. 2 for $E > 0$. An analogous argumentation can be carried out for holes.

To simulate the temporal dynamics, we use Eq. (5), starting with the initial distribution of Eq. (6) at time $t = 0$. Choosing the parameters λ and σ as described above, we calculate time evolutions of occupations for different temperatures T and excitation energies ζ. We are particularly interested in the behavior of thermalization times for excitations below and above the optical phonon threshold.

Figure 3 shows the hot carrier population $P(E, t, T)$ [see Eq. (7)] for excitation energies $\zeta = 0.05, 0.5$ eV and temperatures $T = 0, 10, 100$ K. Below the optical phonon threshold for $\zeta = 0.05$ eV in Figs. 3(a)–3(c), thermalization of the hot carriers takes place on the picosecond timescale via low-energy acoustical phonons. In this excitation range the relaxation time decreases with increasing temperature, because the background equilibrium electron distribution allows excited carriers to scatter increasingly efficiently with the optical phonons [32]. Our thermalization time τ_{th} at $T = 10$ K, as extracted from Fig. 3(b), is around 175 ps. This is lower than the 300 ps reported in Ref. [32] for an excitation energy of 51 meV on an epitaxially grown graphene sample containing around ∼70 layers and arranged over a SiC substrate. Above

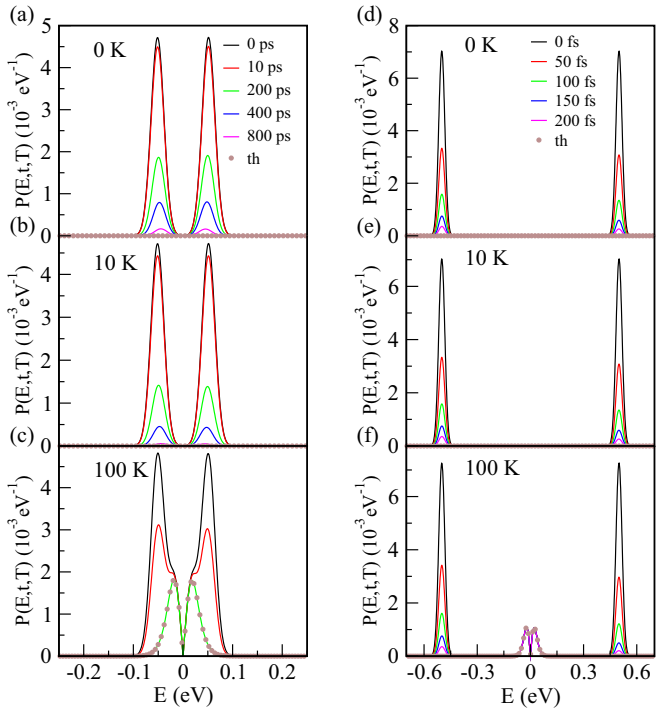

FIG. 3. Time-dependent thermalization of photocarriers at an excitation energy of (a)–(c) 0.05 eV and (d)–(f) 0.5 eV for different temperatures.

the optical phonon threshold, our results in Figs. 3(d)–3(f) predict a weak or almost no temperature dependence of the relaxation time. With $\tau_{th} \approx 60$ fs it takes a value of similar size as the photocarrier isotropization time from Ref. [31], originating from scattering by optical phonons. Our qualitative findings of a strong temperature dependence of τ_{th} below the optical phonon threshold and none above are consistent with the experimental observations in Ref. [32]. The plots in Fig. 3 also demonstrate that the populations of electrons and holes evolve with time quite symmetrically around the Dirac point, confirming that the dynamics of holes are similar to those of electrons.

Due to the extraordinarily high melting temperature of nearly 5000 K predicted theoretically for graphene [46], we extend our analysis of time evolutions to high temperatures $T = 300, 600, 1200, 2000$ K, see Fig. 4. We find carriers to relax at $T = 300$ or 600 K on a 100 fs time scale. At 1200 K this reduces to around 34 fs and is even below 26 fs at 2000 K.

In Fig. 5 we summarize the relaxation times τ_{th}, which we have extracted from the Boltzmann equation combined with our *ab-initio* modeling at different excitation energies and temperatures. For $\zeta = 0.05$ eV the thermalization time decreases with increasing temperature from $T = 0$ to 1200 K by more than three orders of magnitude. In contrast, there is only little change in the relaxation time with temperature for a fixed excitation with $\zeta = 0.4, 0.6, 0.8$ eV above the optical phonon threshold. A slight decrease is seen at the temperatures, where thermal energies are similar to those of optical phonon quanta, i.e., $k_B T \approx \hbar\omega_p$. In addition, for a fixed temperature, relaxation times depend only little on ζ, if the excitation energy is above the optical phonon threshold.

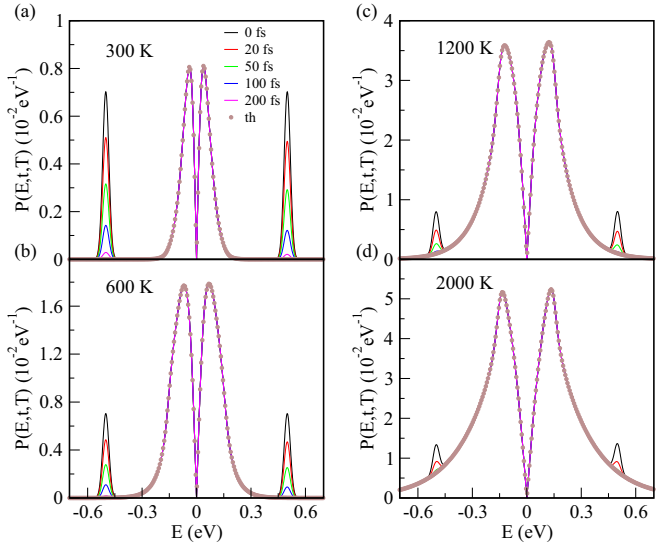

FIG. 4. Same as Fig. 3 at an excitation energy of 0.5 eV for elevated temperatures.

To summarize, taking into account only EP scattering events, we thus observe intriguingly that relaxation times in graphene can span an extraordinary range from 170 ps down to 60 fs, if the temperature is varied and carriers are excited below the optical phonon threshold.

Our predictions can be qualitatively understood by using the concept of a thermalization bottleneck in graphene. Thanks to the high optical phonon energy quanta of about 200 meV [see Fig. 1(d)], the low-energy (THz) electrons cannot relax as fast as the optically excited photocarriers, because at low temperatures (i) the phonon absorption is a very rare process and (ii) the phonon emission requires an empty electron state below the Fermi level, but states below ε_F are almost fully occupied. The relevant thermalization times can be estimated by using our analytical model. We assume

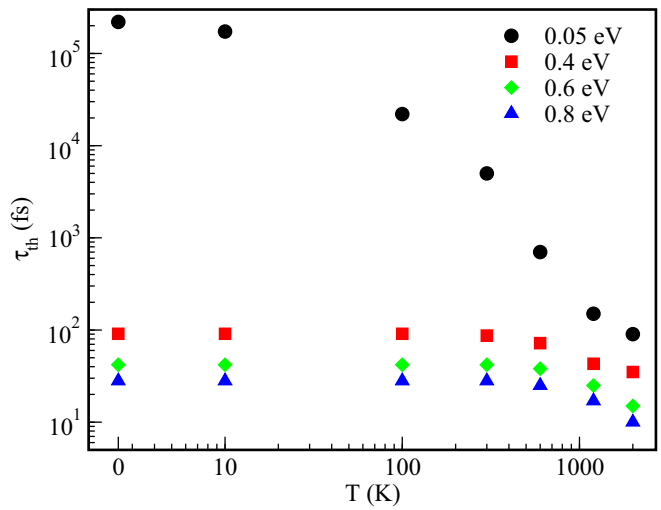

FIG. 5. Thermalization time of the excited carriers, as determined from the Boltzmann equation, as a function of temperature for different excitation energies.

an explicit form for the EP interaction matrix element given by [36]

$$W_p = \frac{\hbar \Delta_p^2 F_p}{2\rho\omega_p}, \tag{21}$$

where Δ_p is the deformation potential for a mode p, F_p is a dimensionless geometric factor, and $\rho = 7.6\times10^{-8}$ g/cm^2 is the mass density. In what follows, we take into account the two most important phonon modes [36], $p = \Gamma, K$, where $F_\Gamma = 1$, $F_K = 1/2$, $\hbar\omega_\Gamma = 197$ meV, $\hbar\omega_K = 157$ meV, and $\Delta_\Gamma = \Delta_0$, $\Delta_K = \sqrt{2}\Delta_0$ with $\Delta_0 = 11$ eV/Å [36]. At $\omega \gg \omega_p$ the thermalization time can be found from Eq. (19) as

$$\tau_{\rm th} = \frac{4\omega_0}{\omega}\frac{\hbar v_{\rm F}^2 \rho}{\Delta_0^2}, \quad \omega \gg \omega_{\Gamma,K}, \tag{22}$$

where $1/\omega_0 = 1/\omega_\Gamma + 1/\omega_K$. Assuming an excitation energy of $\hbar\omega = 1.55$ eV (i.e., a radiation wavelength of 800 nm), we estimate $\tau_{\rm th} \approx 58$ fs. In the opposite limit $\omega \ll \omega_p$ we get from Eq. (20)

$$\tau_{\rm th} = \frac{\hbar v_{\rm F}^2 \rho}{\Delta_0^2}\frac{1}{\exp\left(-\frac{\hbar\omega_\Gamma}{k_{\rm B}T}\right)+\exp\left(-\frac{\hbar\omega_K}{k_{\rm B}T}\right)}, \quad \omega \ll \omega_{\Gamma,K}. \tag{23}$$

Assuming the most relevant temperature of 300 K, we estimate $\tau_{\rm th} \approx 92$ ps.

Our considerations confirm that (i) the thermalization timescales differ at $\omega \ll \omega_p$ and $\omega \gg \omega_p$ by three orders of magnitude at room temperature, (ii) the photocarrier thermalization time strongly depends on temperature at $\omega \ll \omega_p$, whereas at $\omega \gg \omega_p$ it does not, and (iii) in the former case, the thermalization time decreases rapidly with increasing temperature. This is exactly what we see in the summary of the relaxation times $\tau_{\rm th}$ shown in Fig. 5, as determined through our first-principles approach.

IV. SUMMARY AND OUTLOOK

In summary, we have studied the relaxation dynamics of hot carriers in single-layer graphene near and away from the Dirac point subject to the EP interaction. By determining electron and phonon dispersions as well as EP couplings from DFT, our model based on the Boltzmann equation in the RTA contains no free parameters and takes into account contributions from all of the optical as well as acoustical branches in the whole BZ along with the inter- and intraband transitions taking place. In excellent agreement with analytical predictions we find that relaxation times computed with our model are strongly increased, if carriers are excited below the optical phonon energies. In addition, we have shown that the carrier relaxation times depend strongly on temperature for such low excitation energies, while being rather temperature-independent for excitation energies above optical phonon energy quanta. Our results are in agreement with the experimental findings, attributing photocarrier relaxation at different excitation energies to different phonon branches [23,28,32].

DFT results depend on the choice of the exchange-correlation functional. To assess the robustness of DFT-derived electron and phonon dispersions as well as EP couplings, different functionals have been tested in Ref. [55] and compared to the Hartree-Fock and *GW* approximations. While the conelike electron dispersion at the *K* point is consistently reproduced and phonon dispersions are generally found to be in good agreement with experiment, inaccuracies of the EP couplings for the highest optical phonon branch near the *K* point have been corroborated and the *GW* approach has been advocated as a way for making quantitative improvements. While the use of electronic structure methods beyond DFT would certainly be desirable in the future, we expect that more accurate *ab-initio* input parameters will not qualitatively change the results presented here.

The photocarrier thermalization bottleneck could be employed to facilitate the photoexcited electron transport from graphene to a semiconductor across a Schottky barrier [56–58]. Thanks to the longer relaxation time at lower excitation energies, the photocarriers can contribute to the interlayer transport before thermalization is completed, thus improving the photoresponsivity [59]. From the device engineering point of view, the most important assumption made in this work is the absence of a substrate. It might provide additional dielectric screening and unintentional doping, which overall influence the electron-electron scattering contribution neglected here. Moreover, the photocarriers might experience interactions with remote polar surface phonons [36], providing additional EP scattering channels. Since the precise effects caused by a substrate strongly depend on the chosen material and its interface properties, the model should be tailored for each device to make quantitative predictions. Such aspects could be addressed in future work.

ACKNOWLEDGMENTS

D.Y. and F.P. acknowledge financial support from the Carl Zeiss Foundation as well as the Collaborative Research Center (SFB) 767 of the German Research Foundation (DFG). M.T. is supported by the Director's Senior Research Fellowship from the Centre for Advanced 2D Materials at the National University of Singapore (NRF Medium Sized Centre Programme R-723-000-001-281) and thanks the Okinawa Institute of Science and Technology for its hospitality. Part of the numerical modeling was performed using the computational resources of the bwHPC program, namely the bwUniCluster and the JUSTUS HPC facility.

[1] Y. Cao, A. Mishchenko, G. L. Yu, E. Khestanova, A. P. Rooney, E. Prestat, A. V. Kretinin, P. Blake, M. B. Shalom, C. Woods, J. Chapman, G. Balakrishnan, I. V. Grigorieva, K. S. Novoselov, B. A. Piot, M. Potemski, K. Watanabe, T. Taniguchi, S. J. Haigh, A. K. Geim, and R. V. Gorbachev, Quality heterostructures from two-dimensional crystals unstable in air by their assembly in inert atmosphere, Nano Lett. **15**, 4914 (2015).

[2] A. C. Ferrari, F. Bonaccorso, V. Fal'ko, K. S. Novoselov, S. Roche, P. Bøggild, S. Borini, F. H. L. Koppens, V. Palermo, N. Pugno, J. A. Garrido, R. Sordan, A. Bianco, L. Ballerini,

M. Prato, E. Lidorikis, J. Kivioja, C. Marinelli, T. Ryhänen, A. Morpurgo, J. N. Coleman, V. Nicolosi, L. Colombo, A. Fert, M. Garcia-Hernandez, A. Bachtold, G. F. Schneider, F. Guinea, C. Dekker, M. Barbone, Z. Sun, C. Galiotis, A. N. Grigorenko, G. Konstantatos, A. Kis, M. Katsnelson, L. Vandersypen, A. Loiseau, V. Morandi, D. Neumaier, E. Treossi, V. Pellegrini, M. Polini, A. Tredicucci, G. M. Williams, B. H. Hong, J.-H. Ahn, J. M. Kim, H. Zirath, B. J. van Wees, H. van der Zant, L. Occhipinti, A. Di Matteo, I. A. Kinloch, T. Seyller, E. Quesnel, X. Feng, K. Teo, N. Rupesinghe, P. Hakonen, S. R. T. Neil, Q. Tannock, T. Löfwander, and J. Kinaret, Science and technology roadmap for graphene, related two-dimensional crystals, and hybrid systems, Nanoscale **7**, 4598 (2015).

[3] J. Nelson, *The Physics of Solar Cells* (Imperial College Press, London, 2004).

[4] K. S. Novoselov, A. Mishchenko, A. Carvalho, and A. H. Castro Neto, 2D materials and van der Waals heterostructures, Science **353**, aac9439 (2016).

[5] Q. Ma, T. I. Andersen, N. L. Nair, N. M. Gabor, M. Massicotte, C. H. Lui, A. F. Young, W. Fang, K. Watanabe, T. Taniguchi, J. Kong, N. Gedik, F. H. L. Koppens, and P. Jarillo-Herrero, Tuning ultrafast electron thermalization pathways in a van der Waals heterostructure, Nat. Phys. **12**, 455 (2016).

[6] M. T. Mihnev, F. Kadi, C. J. Divin, T. Winzer, S. Lee, C.-H. Liu, Z. Zhong, C. Berger, W. A. de Heer, E. Malić, A. Knorr, and T. B. Norris, Microscopic origins of the terahertz carrier relaxation and cooling dynamics in graphene, Nat. Commun. **7**, 11617 (2016).

[7] J. C. König-Otto, M. Mittendorff, T. Winzer, F. Kadi, E. Malić, A. Knorr, C. Berger, W. A. de Heer, A. Pashkin, H. Schneider, M. Helm, and S. Winnerl, Slow Non-Collinear Coulomb Scattering in the Vicinity of the Dirac Point in Graphene, Phys. Rev. Lett. **117**, 087401 (2016).

[8] D. M. Basko, S. Piscanec, and A. C. Ferrari, Electron-electron interactions and doping dependence of the two-phonon Raman intensity in graphene, Phys. Rev. B **80**, 165413 (2009).

[9] T. Winzer and E. Malić, Impact of Auger processes on carrier dynamics in graphene, Phys. Rev. B **85**, 241404(R) (2012).

[10] T. Winzer, A. Knorr, and E. Malić, Carrier multiplication in graphene, Nano Lett. **10**, 4839 (2010).

[11] T. Plötzing, T. Winzer, E. Malić, D. Neumaier, A. Knorr, and H. Kurz, Experimental verification of carrier multiplication in graphene, Nano Lett. **14**, 5371 (2014).

[12] I. Gierz, F. Calegari, S. Aeschlimann, M. Chávez Cervantes, C. Cacho, R. T. Chapman, E. Springate, S. Link, U. Starke, C. R. Ast, and A. Cavalleri, Tracking Primary Thermalization Events in Graphene with Photoemission at Extreme Time Scales, Phys. Rev. Lett. **115**, 086803 (2015).

[13] T. Winzer, R. Jago, and E. Malić, Experimentally accessible signatures of Auger scattering in graphene, Phys. Rev. B **94**, 235430 (2016).

[14] A. Tomadin, D. Brida, G. Cerullo, A. C. Ferrari, and M. Polini, Nonequilibrium dynamics of photoexcited electrons in graphene: Collinear scattering, Auger processes, and the impact of screening, Phys. Rev. B **88**, 035430 (2013).

[15] T. Winzer and E. Malić, The impact of pump fluence on carrier relaxation dynamics in optically excited graphene, J. Phys.: Condens. Matter **25**, 054201 (2013).

[16] F. Kadi, T. Winzer, A. Knorr, and E. Malić, Impact of doping on the carrier dynamics in graphene, Sci. Rep. **5**, 16841 (2015).

[17] M. Trushin, Collinear scattering of photoexcited carriers in graphene, Phys. Rev. B **94**, 205306 (2016).

[18] P. B. Allen, Theory of Thermal Relaxation of Electrons in Metals, Phys. Rev. Lett. **59**, 1460 (1987).

[19] P. Maldonado, K. Carva, M. Flammer, and P. M. Oppeneer, Theory of out-of-equilibrium ultrafast relaxation dynamics in metals, Phys. Rev. B **96**, 174439 (2017).

[20] S. Ono, Thermalization in simple metals: Role of electron-phonon and phonon-phonon scattering, Phys. Rev. B **97**, 054310 (2018).

[21] S. Sadasivam, M. K. Y. Chan, and P. Darancet, Theory of Thermal Relaxation of Electrons in Semiconductors, Phys. Rev. Lett. **119**, 136602 (2017).

[22] F. Giustino, Electron-phonon interactions from first principles, Rev. Mod. Phys. **89**, 015003 (2017).

[23] D. Brida, A. Tomadin, C. Manzoni, Y. J. Kim, A. Lombardo, S. Milana, R. R. Nair, K. S. Novoselov, A. C. Ferrari, G. Cerullo, and M. Polini, Ultrafast collinear scattering and carrier multiplication in graphene, Nat. Commun. **4**, 1987 (2013).

[24] M. Breusing, S. Kuehn, T. Winzer, E. Malić, F. Milde, N. Severin, J. P. Rabe, C. Ropers, A. Knorr, and T. Elsaesser, Ultrafast nonequilibrium carrier dynamics in a single graphene layer, Phys. Rev. B **83**, 153410 (2011).

[25] C. H. Lui, K. F. Mak, J. Shan, and T. F. Heinz, Ultrafast Photoluminescence from Graphene, Phys. Rev. Lett. **105**, 127404 (2010).

[26] J. Shang, T. Yu, J. Lin, and G. G. Gurzadyan, Ultrafast electron-optical phonon scattering and quasiparticle lifetime in CVD-grown graphene, ACS Nano **5**, 3278 (2011).

[27] J. M. Dawlaty, S. Shivaraman, M. Chandrashekhar, F. Rana, and M. G. Spencer, Measurement of ultrafast carrier dynamics in epitaxial graphene, Appl. Phys. Lett. **92**, 042116 (2008).

[28] J. C. Johannsen, S. Ulstrup, F. Cilento, A. Crepaldi, M. Zacchigna, C. Cacho, I. C. E. Turcu, E. Springate, F. Fromm, C. Raidel, T. Seyller, F. Parmigiani, M. Grioni, and P. Hofmann, Direct View of Hot Carrier Dynamics in Graphene, Phys. Rev. Lett. **111**, 027403 (2013).

[29] I. Gierz, Probing carrier dynamics in photo-excited graphene with time-resolved ARPES, J. Electron Spectrosc. Relat. Phenom. **219**, 53 (2017).

[30] S. Aeschlimann, R. Krause, M. Chávez-Cervantes, H. Bromberger, R. Jago, E. Malić, A. Al-Temimy, C. Coletti, A. Cavalleri, and I. Gierz, Ultrafast momentum imaging of pseudospin-flip excitations in graphene, Phys. Rev. B **96**, 020301(R) (2017).

[31] M. Trushin, A. Grupp, G. Soavi, A. Budweg, D. De Fazio, U. Sassi, A. Lombardo, A. C. Ferrari, W. Belzig, A. Leitenstorfer, and D. Brida, Ultrafast pseudospin dynamics in graphene, Phys. Rev. B **92**, 165429 (2015).

[32] S. Winnerl, M. Orlita, P. Plochocka, P. Kossacki, M. Potemski, T. Winzer, E. Malić, A. Knorr, M. Sprinkle, C. Berger, W. A. de Heer, H. Schneider, and M. Helm, Carrier Relaxation in Epitaxial Graphene Photoexcited Near the Dirac Point, Phys. Rev. Lett. **107**, 237401 (2011).

[33] S. S. Kubakaddi, Interaction of massless Dirac electrons with acoustic phonons in graphene at low temperatures, Phys. Rev. B **79**, 075417 (2009).

[34] R. Bistritzer and A. H. MacDonald, Electronic Cooling in Graphene, Phys. Rev. Lett. **102**, 206410 (2009).

[35] W. K. Tse and S. Das Sarma, Energy relaxation of hot Dirac fermions in graphene, Phys. Rev. B **79**, 235406 (2009).

[36] T. Low, V. Perebeinos, R. Kim, M. Freitag, and P. Avouris, Cooling of photoexcited carriers in graphene by internal and substrate phonons, Phys. Rev. B **86**, 045413 (2012).

[37] E. Malić, T. Winzer, E. Bobkin, and A. Knorr, Microscopic theory of absorption and ultrafast many-particle kinetics in graphene, Phys. Rev. B **84**, 205406 (2011).

[38] R. Kim, V. Perebeinos, and P. Avouris, Relaxation of optically excited carriers in graphene, Phys. Rev. B **84**, 075449 (2011).

[39] J. C. W. Song, M. Y. Reizer, and L. S. Levitov, Disorder-Assisted Electron-Phonon Scattering and Cooling Pathways in Graphene, Phys. Rev. Lett. **109**, 106602 (2012).

[40] E. Malić, T. Winzer, and A. Knorr, Efficient orientational carrier relaxation in optically excited graphene, Appl. Phys. Lett. **101**, 213110 (2012).

[41] S. G. Menabde, H. Cho, and N. Park, Interface defect-assisted phonon scattering of hot carriers in graphene, Phys. Rev. B **96**, 075426 (2017).

[42] M. Calandra and F. Mauri, Electron-phonon coupling and electron self-energy in electron-doped graphene: Calculation of angular-resolved photoemission spectra, Phys. Rev. B **76**, 205411 (2007).

[43] C.-H. Park, F. Giustino, C. D. Spataru, M. L. Cohen, and S. G. Louie, First-Principles Study of Electron Linewidths in Graphene, Phys. Rev. Lett. **102**, 076803 (2009).

[44] C. Ferrante, A. Virga, L. Benfatto, M. Martinati, D. De Fazio, U. Sassi, C. Fasolato, A. K. Ott, P. Postorino, D. Yoon, G. Cerullo, F. Mauri, A. C. Ferrari, and T. Scopigno, Raman spectroscopy of graphene under ultrafast laser excitation, Nat. Commun. **9**, 308 (2018).

[45] S. Wu, W.-T. Liu, X. Liang, P. J. Schuck, F. Wang, Y. R. Shen, and M. Salmeron, Hot phonon dynamics in graphene, Nano Lett. **12**, 5495 (2012).

[46] K. V. Zakharchenko, A. Fasolino, J. H. Los, and M. I. Katsnelson, Melting of graphene: from two to one dimension, J. Phys.: Condens. Matter **23**, 202202 (2011).

[47] P. Giannozzi, S. Baroni, N. Bonini, M. Calandra, R. Car, C. Cavazzoni, D. Ceresoli, G. L. Chiarotti, M. Cococcioni, I. Dabo, A. D. Corso, S. de Gironcoli, S. Fabris, G. Fratesi, R. Gebauer, U. Gerstmann, C. Gougoussis, A. Kokalj, M. Lazzeri, L. Martin-Samos, N. Marzari, F. Mauri, R. Mazzarello, S. Paolini, A. Pasquarello, L. Paulatto, C. Sbraccia, S. Scandolo, G. Sclauzero, A. P. Seitsonen, A. Smogunov, P. Umari, and R. M. Wentzcovitch, QUANTUM ESPRESSO: a modular and open-source software project for quantum simulations of materials, J. Phys.: Condens. Matter **21**, 395502 (2009).

[48] N. Troullier and J. L. Martins, Efficient pseudopotentials for plane-wave calculations, Phys. Rev. B **43**, 1993 (1991).

[49] N. Marzari, A. A. Mostofi, J. R. Yates, I. Souza, and D. Vanderbilt, Maximally localized Wannier functions: Theory and applications, Rev. Mod. Phys. **84**, 1419 (2012).

[50] S. Baroni, S. de Gironcoli, A. D. Corso, and P. Giannozzi, Phonons and related crystal properties from density-functional perturbation theory, Rev. Mod. Phys. **73**, 515 (2001).

[51] J.-A. Yan, W. Y. Ruan, and M. Y. Chou, Phonon dispersions and vibrational properties of monolayer, bilayer, and trilayer graphene: Density-functional perturbation theory, Phys. Rev. B **77**, 125401 (2008).

[52] S. Poncé, E. R. Margine, C. Verdi, and F. Giustino, EPW: Electron-phonon coupling, transport and superconducting properties using maximally localized Wannier functions, Comput. Phys. Commun. **209**, 116 (2016).

[53] A. A. Mostofi, J. R. Yates, G. Pizzi, Y.-S. Lee, I. Souza, D. Vanderbilt, and N. Marzari, An updated version of Wannier 90: A tool for obtaining maximally-localised Wannier functions, Comput. Phys. Commun. **185**, 2309 (2014).

[54] M. Lundstrom, *Fundamentals of Carrier Transport*, 2nd ed. (Cambridge University Press, Cambridge, 2000).

[55] M. Lazzeri, C. Attaccalite, L. Wirtz, and F. Mauri, Impact of the electron-electron correlation on phonon dispersion: Failure of LDA and GGA DFT functionals in graphene and graphite, Phys. Rev. B **78**, 081406(R) (2008).

[56] W. Zhang, C.-P. Chuu, J.-K Huang, C.-H. Chen, M.-L. Tsai, Y.-H. Chang, C.-T. Liang, Y.-Z. Chen, Y.-L. Chueh, J.-H. He, M.-Y. Chou, and L.-J. Li, Ultrahigh-gain photodetectors based on atomically thin graphene-MoS_2 heterostructures, Sci. Rep. **4**, 3826 (2014).

[57] D. De Fazio, I. Goykhman, D. Yoon, M. Bruna, A. Eiden, S. Milana, U. Sassi, M. Barbone, D. Dumcenco, K. Marinov, A. Kis, and A. C. Ferrari, High responsivity, large-area graphene/MoS_2 flexible photodetectors, ACS Nano **10**, 8252 (2016).

[58] M. Massicotte, P. Schmidt, F. Vialla, K. Watanabe, T. Taniguchi, K.-J. Tielrooij, and F. H. Koppens, Photo-thermionic effect in vertical graphene heterostructures, Nat. Commun. **7**, 12174 (2016).

[59] M. Trushin, Theory of photoexcited and thermionic emission across a two-dimensional graphene-semiconductor Schottky junction, Phys. Rev. B **97**, 195447 (2018).